

SIRe-Networks: Skip Connections over Interlaced Multi-Task Learning and Residual Connections for Structure Preserving Object Classification

Danilo Avola^a, Luigi Cinque^a, Alessio Fagioli^a, Gian Luca Foresti^b

^aDepartment of Computer Science, Sapienza University, Via Salaria 113, Rome, 00138, Italy

^bDepartment of Mathematics, Computer Science and Physics, Università di Udine, Via delle Scienze 20, Udine, 33100, Italy

Abstract

Improving existing neural network architectures can involve several design choices such as manipulating the loss functions, employing a diverse learning strategy, exploiting gradient evolution at training time, optimizing the network hyper-parameters, or increasing the architecture depth. The latter approach is a straightforward solution, since it directly enhances the representation capabilities of a network; however, the increased depth generally incurs in the well-known vanishing gradient problem. In this paper, borrowing from different methods addressing this issue, we introduce an interlaced multi-task learning strategy, defined SIRe, to reduce the vanishing gradient in relation to the object classification task. The presented methodology directly improves a convolutional neural network (CNN) by enforcing the input image structure preservation through interlaced auto-encoders, and further refines the base network architecture by means of skip and residual connections. To validate the presented methodology, a simple CNN and various implementations of famous networks are extended via the SIRe strategy and extensively tested on the CIFAR100 dataset; where the SIRe-extended architectures achieve significantly increased performances across all models, thus confirming the presented approach effectiveness.

Keywords: neural network architectures, multi-task learning, deep learning, object classification

1. Introduction

Neural networks and, in particular, deep architectures, perform well on heterogeneous and complex tasks such as medical image analysis [1, 2, 3], person re-identification [4, 5, 6] or emotion recognition [7, 8, 9]. While ever increasing performances are generally obtained by newer systems, improving upon existing architectures can be a daunting experience due, mostly, to the high number of aspects to be accounted for, when designing a new model. Among the many available options, some of the ideas that are being actively explored concern the use of different loss functions, regularization and normalization techniques as well as architectural innovations through, for example, multi-path information processing [10].

Focusing on methodologies exploiting different loss functions, an interesting and effective solution is associated to the use of composite functions [11, 12] to represent, for instance, different outputs to be optimized by a given network, as usually happens in a multi-task learning scenario [13, 14]. Such approaches can be further improved by applying weights to the various loss components, allowing a network to focus more on a specific task among those that are being optimized [15]. Moreover, further architecture refinements might involve employing intermediate loss functions to alter the gradient evolution; a strategy that enables a model to retain better and more meaningful features along the various architecture layers, and allows to obtain improved performances on the addressed task [16]. A different strategy to improve a network performance, often used in conjunction with a custom loss function, lies in-

stead in regularization [17, 18] and normalization techniques [19], where internal weights are modified to enhance a model abstraction capabilities via direct manipulation. Well-known examples of such approaches comprise a dropout strategy [20], to reduce overfitting over the training dataset distribution by omitting random units at training time for more robust input representations [21]; and batch normalization [22, 23], to facilitate deep networks training by normalizing a given batch according to a specific strategy such as the batch mean and variance [24]. While these approaches can alleviate issues such as the vanishing/exploding gradient, or directly improve a network performance, a crucial factor is represented by the architecture internal structure. As a matter of fact, many recent works [10] are focusing on architectural ideas, starting from clever configurations such as the inception layers [16], or skip [25] and residual connections [26]. Indeed, by defining multiple paths inside a given architecture (e.g., inception layer) it is possible to grasp more (or different) details when analyzing an input [27]; whereas using extra connections inside a model allows to strengthen feature propagation and reuse and, consequently, obtain improved performances with respect to simpler networks [28].

Inspired by these solutions, in this paper we focus on the image classification task and present the SIRe methodology, where an interlaced multi-task learning approach is exploited jointly with skip and residual connections to improve a network performances. Specifically, following the rationale behind GoogleNet [16], where intermediate classifications are used to mitigate the vanishing gradient problem, we implement

a simple CNN architecture and extend its design to have intermediate auto-encoders that enable the interlaced multi-task learning. More accurately, these intermediate tasks require the network to recreate the input image so that structural information is preserved. To further enhance both the intermediate and final tasks, we also borrow residual and skip connections from ResNet [26] and U-Net architectures [25], respectively, so that both the classification accuracy and input image reconstruction can obtain higher results with respect to the base model. To evaluate the SIRE methodology, extensive experiments were performed on the CIFAR100 dataset by extending both a simple CNN as well as various well-known models through the presented approach. As demonstrated by the experimental results, through the SIRE extension, the base network is enforced to maintain structural properties of the input image; thus resulting in a significant performance improvement with respect to the base model, and ultimately validating the proposed strategy.

Summarizing, the main contributions of this paper are:

- designing an interlaced multi-task learning approach to directly affect the gradient evolution;
- jointly exploring solutions (i.e., skip/residual connections) to affect a network performances;
- extending the presented SIRE methodology to other well-known architectures.

2. Related Work

Some of the most effective choices, when designing a new network architecture, entail the loss function to be minimized, which is a direct consequence of the task being addressed; possible regularization and normalization techniques, that might enable a network to converge faster on a given task; and the model architecture itself, where defining wrong operations could result in the network diverging from the required task.

Concerning works exploring loss functions [29, 30, 31, 32, 33, 34, 35, 36, 16], an effective strategy is to multiply the loss by a parameter, thus creating a weighted function. This approach directly enables the implementation of adaptive loss strategies, where the function is modified according to a specific rationale. In [29], for instance, the relative magnitude between two subsequent losses is exploited to decide when to update the generative adversarial network (GAN) model; while the authors of [30] leverage such parameters to explore possible loss functions and automatically pick the best one. Employing parameters can be an effective choice, and other approaches follow a similar reasoning by defining ranking losses to obtain a parametric loss function such as in [31] and [32]. Specifically, the former defines a pair-wise ranking loss based on the input image structure, while the latter designs a distributional ranking loss to better separate positive examples from negative ones. A straightforward extension from parametric loss functions is obtained via multi-task loss functions, where different tasks are learned simultaneously. In [33] and [34], for example, the cross-entropy and triplet loss functions, in the former,

and the self/relative samples similarities, in the latter, are optimized jointly to improve the respective network output. A further refinement for multi-task losses can finally be defined by computing intermediate losses, as described by [35] and [16], where losses for similar tasks are computed along the architecture structure; and from which we took inspiration for the proposed interlaced multi-task learning.

Regarding regularization [37, 38, 39, 40] and normalization [41, 42, 43, 44] techniques, they can help to achieve a better input abstraction or faster convergence. In [37], for example, a region dropout is applied to the network input as a data augmentation strategy. The authors of [38], instead, develop an elastic regularization strategy to capture differences among diverse inputs; while in [39], a regularization term is applied to smooth the network output and avoid misclassifying wrong inputs. Regularization procedures can also be defined for internal layers as shown by [40], where a parametrized regularization is designed to improve the model performance by accounting for both network filters and penalty functions. Differently from these methods, [42] and [43] propose normalization strategies to improve the learning capabilities of an architecture. Specifically, [42] employs instance and batch normalizations to retain, respectively, information invariant to appearance changes (e.g., color) and related to content; while [43] defines a group normalization, applied on the filters channels, to improve performances even for lower mini-batch sizes. Input weights can also be normalized, as shown by [44], where the authors also parametrize such weights to speedup the training procedure. Finally, to directly affect data distributions along their architecture, the authors of [41] present an automatic method to learn the best normalization approach for a given layer. Notice that while many significant advances and interesting approaches have been proposed, in this work we employ standard dropout and batch normalization techniques since they are widely accepted procedures.

In relation to approaches considering model architectures [16, 45, 46, 47, 26, 48, 25, 49, 50], several proposals, that also inspired the proposed method, try to improve the optimization task by analyzing and modifying gradient-derived information. More accurately, the authors of [16] implement intermediate losses to reduce the vanishing gradient problem. In [45], losses computed on internal convolution outputs are exploited to improve the input representation. The authors of [46] and [47], instead, show how intermediate losses can reduce the internal representation distance between the components of their respective architectures. Exploiting intermediate loss functions directly affects the gradient evolution during training time; however, more information can also be forwarded inside the architecture through specific connections such as the skip and residual ones. In particular, [26] and [48] apply long skip connections to retain information from previous layers and successfully improve the final output. In [25] and [49], instead, residual connections are implemented to forward more information along the architecture, ultimately improving the underlying network abstraction capabilities.

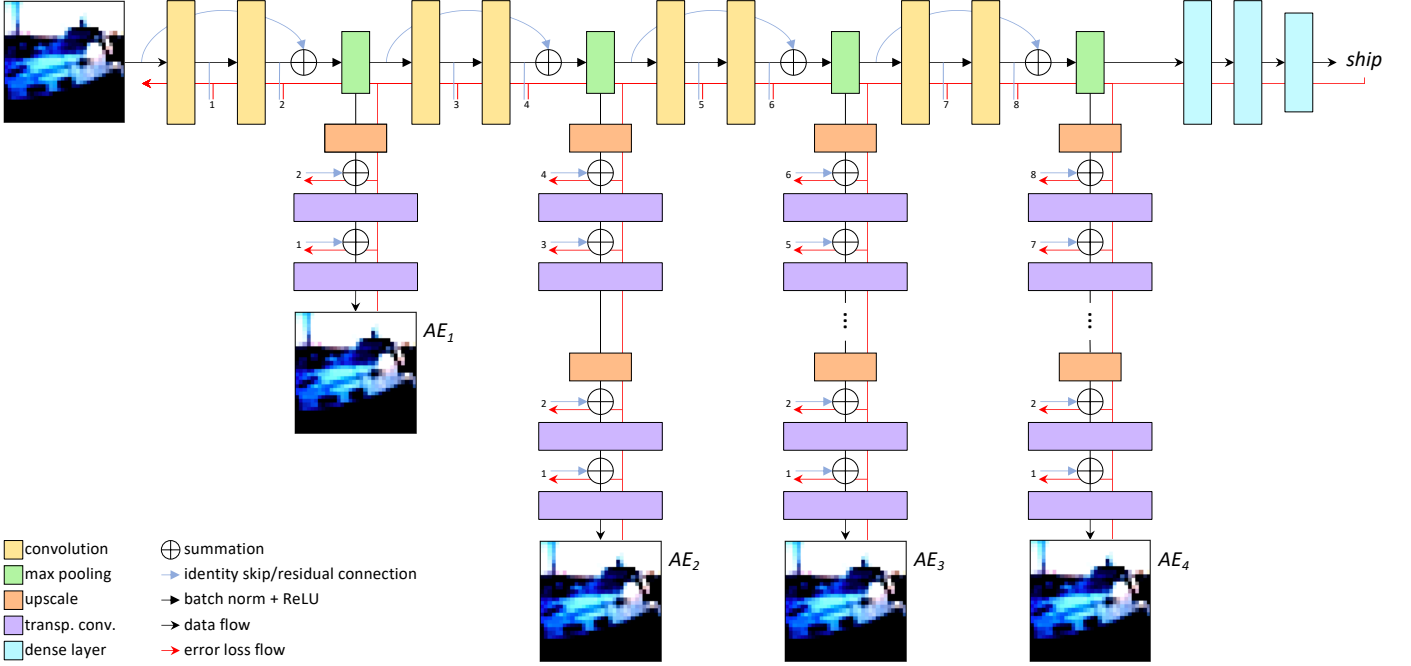


Figure 1: SIRE extended CNN architecture showing the interlaced multi-task learning approach.

3. Method

To present a methodology that consistently improves CNNs performances on the image classification task, we first design a simple network and then extend it through the SIRE technique. In particular, in the proposed approach we implement an interlaced multi-task learning strategy by means of intermediate auto-encoders, to ensure the input image structure is preserved; and further improve the model through long skip and short residual connections, to augment the amount of information forwarded throughout the architecture. The presented SIRE-extended CNN architecture is shown in Fig. 1.

3.1. Base CNN Model

The first step to introduce the SIRE methodology requires the implementation of a simple CNN architecture to be used as a baseline. Specifically, starting from the well-known VGG [51] architecture, we define a less powerful model (i.e., using a fewer number of convolutions and dense units) that can be easily extended and used as a baseline to validate the SIRE adaptation. Notice that the VGG was selected since it has a straightforward implementation, however any other network can be used and extended through the presented methodology, as also highlighted by the experimental results. In more details, the baseline CNN extracts features from an input image through 8 convolutional layers, each followed by a batch normalization, and 4 max pooling layers, placed every 2 convolutions. Subsequently, 3 dense layers are used for the classification task, similarly to the original VGG structure. Concerning the convolutions, in all layers a kernel size $k = 3$ is applied jointly with a padding $p = 1$ to ensure the input shape is retained and reduced only via the max pooling layers. Moreover, the number of filters

generated by the convolutions is doubled after every max pooling operation, starting from 64 in the first convolution (i.e., 64, 128, 256, and 512). Regarding the dense layers, the first two employ the same number of nodes (i.e., 1024) and a dropout strategy to avoid overfitting over the training dataset; while the third one contains m units, where $|m|$ corresponds to the number of classes to be recognized. Finally, the activation function applied to all $l - 1$ layers is the rectified linear activation function (ReLU), while the last one uses a softmax function to obtain a probability distribution for the input classification.

3.2. SIRE Extension

Core component behind the SIRE adaptation lies in the interlaced multi-task learning strategy, where intermediate auto-encoders are used to extend the architecture and manipulate the gradient. Intuitively, these auto-encoders are tasked with the input image reconstruction as to preserve its attributes inside the convolutions. Notice that by defining such components, the base architecture effectively performs an interlaced multi-task learning, where the original task is the object classification, while the intermediate ones correspond to the input reconstruction. Furthermore, the rationale behind this approach is two-fold. First, it can alleviate the vanishing gradient problem, as was also suggested by the authors of [16], by defining extra tasks that directly inject additional gradient error inside the model at training time. Second, it naturally enforces the network to preserve meaningful input characteristics (i.e., features) along the whole architecture; therefore providing an improved input abstraction to the classifier. In particular, an auto-encoder is built upon each max pooling layer, i.e., AE_i , with $i \in [1, \dots, |max_pool_layers|]$, since they correspond to most of the information loss due to the dimensionality reduction.

Moreover, in order to allow the correct output generation, every AE follows the underlying architecture structure. Specifically, they invert all max pooling operations and convolution layers, through the upscaling strategy proposed in [25] and transposed convolutional layers [52], respectively. For example, as shown in Fig. 1, the auto-encoder built upon the third max pooling layer will perform 3 upscale operations, to reach the original input image size, interleaved by 6 transposed convolutions (i.e., 2 layers after each upscale) employing the same k and p of the convolutional layers to correctly reinterpret the input.

Attaching interleaved tasks via auto-encoders helps to inject gradient error during the backpropagation algorithm execution. However, since the intermediate tasks greatly differ from the final output in both structure and purpose, a further enhancement is implemented to improve the information forwarded inside the architecture by means of skip and residual connections. In more details, short residual connections are applied before each max pool operation and connect two subsequent convolutions with their input, similarly to [26]; while long skip connections bond a given convolution with its corresponding transposed convolution in the auto-encoder, to compensate with missing information derived from both the max pool and upscale operations. Notice that neither short residual and long skip connections increase the number of parameters or network complexity, since they are implemented through identity maps and simple summations in accordance with the findings of [26]; therefore resulting in great tools for information propagation and performance improvement.

3.3. Loss Function

A SIRE extended network addressing the classification task, can still be trained end-to-end via classical algorithms such as the stochastic gradient descent (SGD) with backpropagation. However, a specific loss function needs to be implemented to fully leverage the presented methodology and correctly merge the intermediate objectives with the original task. Intuitively, by exploiting the computational graph associated to the network structure, each auto-encoder will focus on specific portions of the architecture and automatically increase the gradient error throughout the model. For instance, observing Fig. 1, the first auto-encoder will affect only the first two convolutions, while the fourth one will influence the whole architecture during the error backpropagation. What is more, through the backpropagation, the interlaced multi-task methodology enforces to retain structural information on the input since all auto-encoders try to correctly reconstruct the original image. Formally, given a SIRE extended network with several auto-encoders AE , the interlaced multi-task loss function is computed as:

$$\mathcal{L} = -\frac{1}{m} \sum_{i=1}^m y_i \log(\hat{y}_i) + \lambda \sum_{AE} \left(\frac{1}{n} \sum_{j=1}^n (AE_{o_j} - x_j)^2 \right), \quad (1)$$

where the first term is a cross-entropy loss computed over the m classes, used to classify the input image; while the second member corresponds to a mean squared error loss for each available auto-encoder AE , evaluating the input image reconstruction. In

particular, AE_{o_j} and x_j indicate, respectively, the j -th pixel predicted output of a given auto-encoder AE and input image (i.e., ground truth for the intermediate task); n represents the input image number of pixels; while λ is an hyperparameter regulating the interlaced multi-task loss strength over the underlying architecture, empirically set to 0.2 in this work. Notice that due to the diverse nature of the intermediate tasks and final output, a too high value of λ might result in the network focusing on the input reconstruction instead of the classification, as demonstrated by the performed experiments.

4. Experiments

Extensive experiments were carried out to fully evaluate the proposed SIRE methodology. The dataset and test protocol employed to ensure sound results across all tests, are described in Section 4.1. Quantitative and qualitative ablation studies are instead discussed in Section 4.2, where in depth details on the described approach are provided. Finally, experiments on SIRE extended networks are presented in Section 4.3, to highlight the methodology effectiveness.

4.1. Implementation Details

All experiments, including ablation studies on the SIRE-CNN and the SIRE extension to other literature networks, were performed on the CIFAR100 [53] dataset. This collection contains 60000 32×32 RGB images spanning over 100 classes. In particular, there are 500 training and 100 test images per class, resulting in the training and test sets containing 50000 and 10000 images, respectively. Moreover, in this work we further split the training set to retain 50 images per class to define a validation set. Therefore, the final collections count 45000, 5000, and 10000 samples, for the training, validation, and test sets.

Regarding the various experimental settings, all models were trained following a protocol similar to [54]. Specifically, each network was trained for 200 epochs using the SGD algorithm, with an initial learning rate lr set to 0.1, a weight decay of $5e-4$, and a Nesterov momentum of 0.9. Moreover, a scheduler was also implemented to divide the lr by 5 at epochs 60, 120, and 160, so that the gradient update speed would be gradually reduced. Furthermore, a simple data augmentation strategy was also applied by means of random horizontal flips. Finally, for all models, the weights associated to the epoch with the highest validation set performances were used to compute the reported results on the test set. Notice that for all experiments, the metrics of choice were the top-1(-5) error percentage, which is computed as $1 - \text{rank \#1(-5) accuracy}$; and where lower scores correspond to better performances.

Lastly, all networks were implemented through the PyTorch framework and tests were performed using a single GPU, i.e., a GeForce GTX 1070 with 8GB of RAM.

4.2. Ablation Studies

The first experiment explores the sheer effectiveness of each SIRE component, i.e., the skip connections (S), interlaced

Model	Top-1 Error%	Top-5 Error%	Params	Training Time
Baseline	35.44	12.11	7.9M	$\approx 124'$
Re-CNN	32.21	10.78	7.9M	$\approx 132'$
I-CNN	29.05	9.33	14.0M	$\approx 205'$
IRe-CNN	27.65	8.97	14.0M	$\approx 207'$
SI-CNN	27.83	9.01	14.0M	$\approx 206'$
SIRE-CNN	26.15	8.22	14.0M	$\approx 212'$

Table 1: Ablation study on SIRE components. S, I, and Re, indicate skip connections, interleaved multi-task learning, and residual connections, respectively. All models employ the same CNN, which is also reported as Baseline.

multi-task learning (I), and residual connections (Re). Performances are summarized in Table 1. As shown, all configurations can achieve significant top-1 and top-5 classification performances, with the former obtaining substantially higher gains, independently from the SIRE component. Notice that this score increment difference is most entirely attributable to classes having similar characteristics (e.g., girl and boy) that can be lost due to the small image format of the dataset, but that would still allow for the correct category to be selected among the first 5 most probable classes. What is more, while each extension offers a performance boost, even when applied as a standalone solution, they affect different aspects of the underlying architecture and should, therefore, be used jointly. In particular, the Re unit provides a direct upgrade to the base CNN final classification by forwarding residual information along its architecture. The I component offers the highest error reduction among the single extensions, by focusing on the input image structure preservation; however, it also requires more parameters to be implemented and, as a consequence, more time to be trained (i.e., $\approx 1.7\times$ more time with respect to the base network). Finally, the S component directly refines the interleaved multi-task outputs by forwarding information to the various AEs and, therefore, also reduces the final network error. This intermediate output refinement can be clearly observed in Fig. 2. As shown, without implementing skip connections, the max pool and upsample operations result in information loss, especially when moving toward the deeper auto-encoders that, consequently, reconstruct blurred images. Through the S components, instead, all lost input information is retrieved and almost perfect input reconstruction is achieved (i.e., MSE loss $\leq 3e-6$). Nevertheless, while skip connections improve the AEs output and enforce the input image structure preservation, they do not guarantee a comprehensive class abstraction. As a matter of fact, the last two images (i.e., lion and lamp) are correctly classified only in the top-5 most probable classes, even though they are still correctly recreated.

The second experiment investigates the λ -value effects on the training task; where $\lambda = 0$ removes the interleaved auto-encoders, while $\lambda \geq 1.0$ takes into account the entire AE error. Several significant results for these tests are reported in Table 2. As can be seen, using a small λ -value (i.e., ≤ 0.2) enables the underlying CNN to extract more meaningful features and increase its classification performances. Differently,

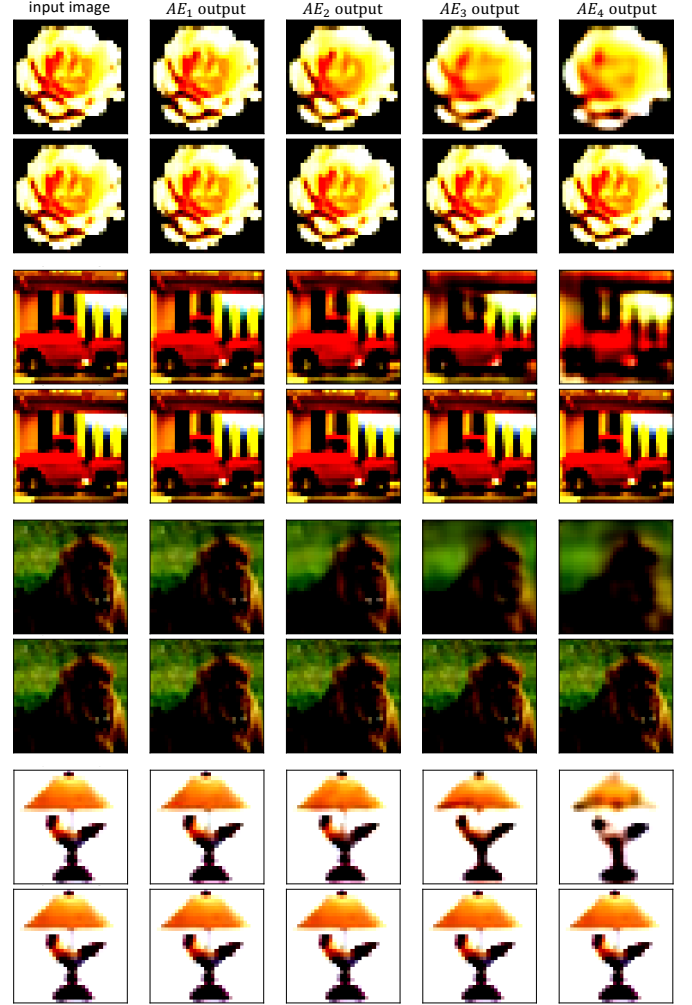


Figure 2: Skip connections effect on the auto-encoders output. The first row for each image corresponds to the IRe-CNN model, while the second row to the full SIRE-CNN. From left to right, the input image and the four autoencoder outputs.

by increasing λ over the value 0.2, which was empirically found to be the best amount, the underlying CNN error increases until the classification task does not reach convergence anymore, i.e., the CNN always outputs the same class for any given input; thus resulting in the reported 99% error. The rationale behind this outcome can easily be explained by the backpropagated gradient derived from the interleaved auto-encoders. Specifically, for higher λ -values, the loss function focuses on the input image reconstruction and all internal parameters are modified to address this task that should, instead, support the classification one. Nevertheless, by choosing an opportune λ -value (i.e., $\lambda = 0.2$), the right amount of AE error is backpropagated and a performance increase is obtained; indicating that intermediate and diverse tasks (e.g., the proposed image reconstruction) can help to improve the original one.

The third experiment analyses the amount of information each AE provides to the classification task. An evaluation comprising all possible AE combinations, where each i -th AE_i corresponds to those presented in Fig. 1, is reported in Table 3.

Model	λ -Value	Top-1 Error%	Top-5 Error%
Baseline	-	32.21	10.78
SIRe-CNN	0.1	31.87	10.66
SIRe-CNN	0.2	26.15	8.22
SIRe-CNN	0.5	99.00	99.00
SIRe-CNN	1.0	99.00	99.00

Table 2: Ablation study on λ -value effects. The Baseline model corresponds to the Re-CNN of Table 1.

As shown, by implementing more *AEs* (e.g., $AE_{1,2,4}$) the error decreases sensibly, however more parameters and training time are required as a trade-off for the improved performance. What is more, this compromise is more marked for models employing deeper *AEs* (i.e., AE_3 and AE_4) since more upscale and transposed convolution operations have to be performed to correctly recreate the input. Nevertheless, redundancy by means of shallower *AEs* (i.e., AE_1 and AE_2) enables for relevant information to be extracted by the base-CNN and allows to obtain better results on the final classification task; thus encouraging the application of multiple *AEs* even though deeper ones have slightly better performance gains. The rationale behind this behaviour is also highlighted in Fig. 3, where the convolutional layers gradient flow is reported for each *AE*, as well as the whole SIRe-CNN and base CNN models. As can be seen, while each *AE* mitigates the vanishing gradient problem (i.e., more error is propagated along the architecture), they still do not solve it entirely and therefore support the chosen redundancy for a better error propagation. As a matter of fact, the gradient flow for the SIRe-CNN is more uniform across all convolutions, while it shows error peaks when analyzing the single *AEs* (e.g., SIRe- AE_1 has such a peak in convolutional layers 1 and 2). Notice that applying different λ -values to each autoencoder to address the vanishing gradient does not solve the issue due to diminished returns on far layers (e.g., the first convolution is slightly affected by AE_4 in comparison with AE_1). Moreover, the same issue described in the λ -value ablation study (i.e., failed convergence) also applies to the single components, forcing the final value to be close to the selected $\lambda = 0.2$ to obtain a significant performance boost.

Summarizing, each component of the SIRe methodology can improve the base CNN performance even as a standalone solution. Moreover, provided an opportune λ -value is selected, implementing multiple intermediate tasks further boosts the original network performance; demonstrating the SIRe extension effectiveness.

4.3. SIRe-Networks Performance Evaluation

To complete the SIRe methodology evaluation, several networks were extended to implement the interlaced multi-task learning approach. Notice that while the proposed method can be theoretically applied to any given model performing classification, we selected a few well-known and good performing architectures to both validate the methodology as well as to provide more insights on its strengths and weaknesses. In particular, the chosen models are the VGG [51], from which our base

Model	Top-1 Error%	Top-5 Error%	Params	Training Time
Baseline	35.44	12.11	7.9M	$\approx 124'$
SIRe- AE_1	32.54	11.41	7.9M	$\approx 125'$
SIRe- AE_2	32.28	11.29	8.2M	$\approx 126'$
SIRe- AE_3	32.04	11.13	9.0M	$\approx 133'$
SIRe- AE_4	31.89	11.00	12.6M	$\approx 195'$
SIRe- $AE_{1,2}$	30.31	10.27	8.2M	$\approx 127'$
SIRe- $AE_{1,3}$	30.12	10.05	9.1M	$\approx 134'$
SIRe- $AE_{1,4}$	30.07	9.71	12.6M	$\approx 197'$
SIRe- $AE_{2,3}$	30.09	9.70	9.3M	$\approx 138'$
SIRe- $AE_{2,4}$	29.91	9.39	12.8M	$\approx 199'$
SIRe- $AE_{3,4}$	29.55	9.31	13.7M	$\approx 208'$
SIRe- $AE_{1,2,3}$	26.99	8.92	9.3M	$\approx 141'$
SIRe- $AE_{1,2,4}$	26.71	8.24	12.9M	$\approx 200'$
SIRe- $AE_{2,3,4}$	26.32	8.23	14.0M	$\approx 211'$
SIRe-CNN	26.15	8.22	14.0M	$\approx 212'$

Table 3: Ablation study on information propagated by the various autoencoders defined in the SIRe methodology.

CNN takes inspiration, with its VGG16 and VGG19 variants employing the batch normalization; ResNet [26], that already implements short residual connections, with its ResNet34 and ResNet50 implementations; and GoogleNet [16], which reiterates the classification task in its internal layers to mitigate the vanishing gradient and reinforce the final output.

To correctly apply the SIRe methodology to the aforementioned networks, the various SIRe components need to be integrated with the underlying architectures that might, on the other hand, have articulated solutions (e.g., inception layers). Notice that analogously to the presented CNN, in this work we invert all operations in a given *AE* path of an extended network to recreate the input image, i.e., we pair each max pooling layer with an upsampling one, and convolutions with their transposed implementation; short residual and long skip connections are subsequently implemented to increase the information propagation. In particular, concerning VGG models, the SIRe extension follows the same approach proposed for the CNN in Fig. 1, inverting each path in conjunction with the max pooling operations. Similarly, short residual connections and long skip connections are subsequently defined to obtain the full SIRe-VGG architecture. Notice that VGG models also implement a fifth max pool operation to create a single 512-D feature vector used for classification, therefore, there will be a fifth *AE* for these extended models (i.e., SIRe-VGG16 and SIRe-VGG19). In relation to the ResNet architectures, the base models already implement residual connections through residual blocks. Consequently, to obtain their SIRe version, the backbone network is extended only via the interlaced multi-task learning and long skip connections. Notice that residual blocks are employed also in the various *AE* but with transposed convolutions to fully invert the various operations. Moreover, similarly to VGG models, the ResNet architecture also implements 5 down sampling operations, resulting in a fifth *AE* for both extended models

Model	λ -value	Top-1 Error%	Top-5 Error%	Params	Training Time
Baseline-CNN	-	35.44	12.11	7.9M	$\approx 119'$
SIRe-CNN	0.20	26.15	8.22	14.0M	$\approx 202'$
VGG16	-	29.18	13.01	138.3M	$\approx 187'$
SIRe-VGG16	0.20	23.02	10.00	160.9M	$\approx 336'$
VGG19	-	28.29	11.43	143.6M	$\approx 195'$
SIRe-VGG19	0.20	22.67	9.62	176.8M	$\approx 370'$
ResNet34	-	22.17	6.29	21.8M	$\approx 412'$
SIRe-ResNet34	0.21	18.35	6.01	50.4M	$\approx 698'$
ResNet50	-	21.26	5.41	25.6M	$\approx 433'$
SIRe-ResNet50	0.21	17.89	5.32	59.4M	$\approx 721'$
GoogLeNet	-	22.92	6.61	13.0M	$\approx 317'$
SIRe-GoogLeNet	0.19	18.21	5.99	17.0M	$\approx 380'$

Table 4: Comparison between several literature networks and their SIRe-extended version.

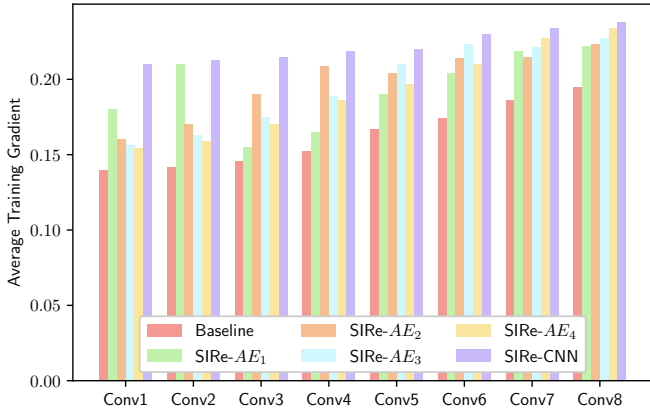


Figure 3: Average gradient flow inside the 8 convolutional layers for the baseline CNN; auto-encoders AE_1 , AE_2 , AE_3 , AE_4 in standalone solutions; and SIRe-CNN. All values are computed during the corresponding model training phase.

(i.e., SIRe-ResNet34 and SIRe-ResNet50). Lastly, regarding the GoogLeNet model, AE s were once again attached to each of the 4 max pool operations. Furthermore, inception layers were only partially inverted due to their internal structure. Specifically, all convolutions were substituted via their transposed, while the max pooling operation inside each AE inception layer was left as is for two reasons. First, the operation is only partially invertible, since it loses information about non-maxima values; and second, in the original inception implementation the filter size remains fixed, therefore allowing for the same max pool operation to be employed in the inverted inception layer. Notice, moreover, that the auxiliary tasks were left untouched, thus resulting in 4 interlaced AE s, used for the input image structure preservation, and 2 original internal classifications for a total of 6 internal tasks in the extended model (i.e., SIRe-GoogLeNet).

Concerning the evaluation, results for the base models and their SIRe extension is reported in Table 4. The same test protocol described in Section 4.1 is employed to assess all models and provide a fair comparison. As shown, the presented methodology improves all architectures for both top-1 and top-

5 error metrics; with the former obtaining sensibly higher performance gains (i.e., up to 9% and 3% for top-1 and top-5 metrics, respectively). Similarly to the ablation studies, this discrepancy is easily explained by samples moving from a top-5 selection to a top-1 due to the input image structure preservation derived from the AE s, i.e., a given object was already close to being correctly classified and the extra information allowed for the right decision. What is more, while not reported due to negligible results differences, a good performing λ -value is close to 0.2 also for other SIRe extended networks; further confirming both the findings and the discussion presented in Section 4.2. On a different note, while SIRe-extended networks can perform better with respect to their original implementation, there is a significant trade-off between the improved performance and the number of parameters required to implement the SIRe methodology. Notice, however, that all extra parameters are employed to exclusively address the input image reconstruction task, therefore highlighting the proposed extension effectiveness in improving the original addressed task. Furthermore, the extra parameters amount is highly dependent on the underlying architecture. For instance, SIRe-ResNet50 requires a $\approx 132\%$ parameter number increase, while SIRe-VGG19 only a $\approx 23\%$ increment to implement the SIRe methodology. Observe that this lower amount, in correlation with the total parameter quantity shown in Table 4, is a consequence of most parameters being associated to the classifier in the original VGG19 architecture. Notice also that the internal structure of a given network directly affects the total training time. For instance, even though the VGG19 has roughly 6x the number of parameters of a ResNet50 (i.e., 143M against 25M), it still requires less time to be fully trained according to the presented test protocol. Nevertheless, the trainable parameter number also influences the time required to train a given network and, consequently, its SIRe extension (e.g., up to $\approx 70\%$ for the selected models). Indeed, while the proposed SIRe extension can be theoretically applied to any network performing classification, further investigations on possible reduced interlaced multi-task implementations (e.g., less AE layers) are required to simplify, without loss of generality, the SIRe extended network training procedure; an improvement that would enable the presented methodology

application to the ever more complex architectures being developed, but which is left as future work.

5. Conclusion

In this paper we introduced the SIRE methodology, that allows to improve the classification capabilities of a given network by exploiting the input image structure preservation through an interlaced multi-task learning strategy; which is further refined via long skip and short residual connections. Moreover, both strengths and shortcomings for the proposed approach, i.e., a significant classification performance boost and a required training time increase, were presented and discussed through several ablation studies. Finally, the SIRE methodology was also applied to different well-known literature works, validating the proposed strategy by means of improved performances on all of the extended architectures.

As future work we plan to investigate possible strategies to reduce the amount of parameters required to implement the SIRE approach in even more complex architectures, without any loss of generality for the input image reconstruction and structure preservation rationale. Furthermore, other extensive experiments will also be performed to explore the effects of different and multiple interlaced tasks with respect to the classification one, to ultimately obtain ever improving feature abstractions.

Acknowledgments

This work was supported in part by the MIUR under grant “Departments of Excellence 2018–2022” of the Department of Computer Science of Sapienza University.

References

- [1] M. Gridach, Pydinnet: Pyramid dilated network for medical image segmentation, *Neural Networks* 140 (2021) 274–281.
- [2] I. Oksuz, J. R. Clough, B. Ruijsink, E. P. Anton, A. Bustin, G. Cruz, C. Prieto, A. P. King, J. A. Schnabel, Deep learning-based detection and correction of cardiac mr motion artefacts during reconstruction for high-quality segmentation, *IEEE Transactions on Medical Imaging* 39 (12) (2020) 4001–4010.
- [3] D. Avola, L. Cinque, A. Fagioli, S. Filetti, G. Grani, E. Rodolà, Multi-modal feature fusion and knowledge-driven learning via experts consult for thyroid nodule classification, *IEEE Transactions on Circuits and Systems for Video Technology* preprint (2021) 1–8.
- [4] J. Wu, Y. Yang, Z. Lei, J. Wang, S. Z. Li, P. Tiwari, H. M. Pandey, An end-to-end exemplar association for unsupervised person re-identification, *Neural Networks* 129 (2020) 43–54.
- [5] Y. Tang, X. Yang, N. Wang, B. Song, X. Gao, Person re-identification with feature pyramid optimization and gradual background suppression, *Neural Networks* 124 (2020) 223–232.
- [6] D. Avola, L. Cinque, A. Fagioli, G. L. Foresti, D. Pannone, C. Picciarelli, Bodyprint—a meta-feature based lstm hashing model for person re-identification, *Sensors* 20 (18) (2020) 5365.
- [7] Z. Zhao, Q. Li, Z. Zhang, N. Cummins, H. Wang, J. Tao, B. W. Schuller, Combining a parallel 2d cnn with a self-attention dilated residual network for ctc-based discrete speech emotion recognition, *Neural Networks* 141 (2021) 52–60.
- [8] Z. Liang, S. Oba, S. Ishii, An unsupervised eeg decoding system for human emotion recognition, *Neural Networks* 116 (2019) 257–268.
- [9] D. Avola, L. Cinque, A. Fagioli, G. L. Foresti, C. Massaroni, Deep temporal analysis for non-acted body affect recognition, *IEEE Transactions on Affective Computing* 0 (2020) 1–12.
- [10] A. Khan, A. Sohail, U. Zahoor, A. S. Qureshi, A survey of the recent architectures of deep convolutional neural networks, *Artificial Intelligence Review* 53 (8) (2020) 5455–5516.
- [11] K. Zhang, W. Luo, L. Ma, W. Liu, H. Li, Learning joint gait representation via quintuplet loss minimization, in: *Proceedings of the IEEE/CVF Conference on Computer Vision and Pattern Recognition (CVPR)*, 2019, pp. 4700–4709.
- [12] S. Kim, D. Kim, M. Cho, S. Kwak, Proxy anchor loss for deep metric learning, in: *Proceedings of the IEEE/CVF Conference on Computer Vision and Pattern Recognition (CVPR)*, 2020, pp. 3238–3247.
- [13] Z. Chen, L. Zhu, L. Wan, S. Wang, W. Feng, P.-A. Heng, A multi-task mean teacher for semi-supervised shadow detection, in: *Proceedings of the IEEE/CVF Conference on Computer Vision and Pattern Recognition (CVPR)*, 2020, pp. 5611–5620.
- [14] Z. Tang, M. Naphade, S. Birchfield, J. Tremblay, W. Hodge, R. Kumar, S. Wang, X. Yang, Pamtri: Pose-aware multi-task learning for vehicle re-identification using highly randomized synthetic data, in: *Proceedings of the IEEE/CVF International Conference on Computer Vision (ICCV)*, 2019, pp. 210–220.
- [15] D. Park, S. Hong, B. Han, K. M. Lee, Continual learning by asymmetric loss approximation with single-side overestimation, in: *Proceedings of the IEEE/CVF International Conference on Computer Vision (ICCV)*, 2019, pp. 3335–3344.
- [16] C. Szegedy, W. Liu, Y. Jia, P. Sermanet, S. Reed, D. Anguelov, D. Erhan, V. Vanhoucke, A. Rabinovich, Going deeper with convolutions, in: *Proceedings of the IEEE Conference on Computer Vision and Pattern Recognition (CVPR)*, 2015, pp. 1–9.
- [17] Z. Luo, S. Cai, G. Chen, J. Gao, W.-C. Lee, K. Y. Ngiam, M. Zhang, Improving data analytics with fast and adaptive regularization, *IEEE Transactions on Knowledge and Data Engineering* 33 (2) (2021) 551–568.
- [18] K. Liu, W. Tang, F. Zhou, G. Qiu, Spectral regularization for combating mode collapse in gans, in: *Proceedings of the IEEE/CVF International Conference on Computer Vision (ICCV)*, 2019, pp. 6382–6390.
- [19] R. Zhang, Z. Peng, L. Wu, Z. Li, P. Luo, Exemplar normalization for learning deep representation, in: *Proceedings of the IEEE/CVF Conference on Computer Vision and Pattern Recognition (CVPR)*, 2020, pp. 12726–12735.
- [20] N. Srivastava, G. Hinton, A. Krizhevsky, I. Sutskever, R. Salakhutdinov, Dropout: a simple way to prevent neural networks from overfitting, *The Journal of Machine Learning Research* 15 (1) (2014) 1929–1958.
- [21] Z. Huang, Y. Xu, J. Shi, X. Zhou, H. Bao, G. Zhang, Prior guided dropout for robust visual localization in dynamic environments, in: *Proceedings of the IEEE/CVF International Conference on Computer Vision (ICCV)*, 2019, pp. 2791–2800.
- [22] M. Binkowski, D. Hjelm, A. Courville, Batch weight for domain adaptation with mass shift, in: *Proceedings of the IEEE/CVF International Conference on Computer Vision (ICCV)*, 2019, pp. 1844–1853.
- [23] S. Cui, S. Wang, J. Zhuo, L. Li, Q. Huang, Q. Tian, Towards discriminability and diversity: Batch nuclear-norm maximization under label insufficient situations, in: *Proceedings of the IEEE/CVF Conference on Computer Vision and Pattern Recognition (CVPR)*, 2020, pp. 3941–3950.
- [24] S. Ioffe, C. Szegedy, Batch normalization: Accelerating deep network training by reducing internal covariate shift, in: *Proceedings of the International Conference on Machine Learning (ICML)*, 2015, pp. 448–456.
- [25] O. Ronneberger, P. Fischer, T. Brox, U-net: Convolutional networks for biomedical image segmentation, in: *Proceedings of the International Conference on Medical Image Computing and Computer-Assisted Intervention (MICCAI)*, 2015, pp. 234–241.
- [26] K. He, X. Zhang, S. Ren, J. Sun, Deep residual learning for image recognition, in: *Proceedings of the IEEE Conference on Computer Vision and Pattern Recognition (CVPR)*, 2016, pp. 770–778.
- [27] H. Wang, J. Peng, Y. Zhao, X. Fu, Multi-path deep cnns for fine-grained car recognition, *IEEE Transactions on Vehicular Technology* 69 (10) (2020) 10484–10493.
- [28] G. Huang, Z. Liu, L. Van Der Maaten, K. Q. Weinberger, Densely connected convolutional networks, in: *Proceedings of the IEEE Conference on Computer Vision and Pattern Recognition (CVPR)*, 2017, pp. 4700–4708.
- [29] X. Ouyang, Y. Chen, G. Agam, Accelerated wgan update strategy with loss change rate balancing, in: *Proceedings of the IEEE/CVF Winter Conference on Applications of Computer Vision (WACV)*, 2021, pp. 2546–

- 2555.
- [30] C. Li, X. Yuan, C. Lin, M. Guo, W. Wu, J. Yan, W. Ouyang, Am-lfs: Automl for loss function search, in: *Proceedings of the IEEE/CVF International Conference on Computer Vision (ICCV)*, 2019, pp. 8410–8419.
 - [31] K. Xian, J. Zhang, O. Wang, L. Mai, Z. Lin, Z. Cao, Structure-guided ranking loss for single image depth prediction, in: *Proceedings of the IEEE/CVF Conference on Computer Vision and Pattern Recognition (CVPR)*, 2020, pp. 611–620.
 - [32] Q. Qian, L. Chen, H. Li, R. Jin, Dr loss: Improving object detection by distributional ranking, in: *Proceedings of the IEEE/CVF Conference on Computer Vision and Pattern Recognition (CVPR)*, 2020, pp. 12164–12172.
 - [33] F. Zheng, C. Deng, X. Sun, X. Jiang, X. Guo, Z. Yu, F. Huang, R. Ji, Pyramidal person re-identification via multi-loss dynamic training, in: *Proceedings of the IEEE/CVF Conference on Computer Vision and Pattern Recognition (CVPR)*, 2019, pp. 8514–8522.
 - [34] X. Wang, X. Han, W. Huang, D. Dong, M. R. Scott, Multi-similarity loss with general pair weighting for deep metric learning, in: *Proceedings of the IEEE/CVF Conference on Computer Vision and Pattern Recognition (CVPR)*, 2019, pp. 5022–5030.
 - [35] Z. Chen, H. Zhou, J. Lai, L. Yang, X. Xie, Contour-aware loss: Boundary-aware learning for salient object segmentation, *IEEE Transactions on Image Processing* 30 (2020) 431–443.
 - [36] Y. R. Choi, R. M. Kil, Face video retrieval based on the deep cnn with rbf loss, *IEEE Transactions on Image Processing* 30 (2020) 1015–1029.
 - [37] S. Yun, D. Han, S. J. Oh, S. Chun, J. Choe, Y. Yoo, Cutmix: Regularization strategy to train strong classifiers with localizable features, in: *Proceedings of the IEEE/CVF International Conference on Computer Vision (ICCV)*, 2019, pp. 6023–6032.
 - [38] Y. Zhong, W. Deng, Adversarial learning with margin-based triplet embedding regularization, in: *Proceedings of the IEEE/CVF International Conference on Computer Vision (ICCV)*, 2019, pp. 6549–6558.
 - [39] J. C. Nascimento, G. Carneiro, One shot segmentation: unifying rigid detection and non-rigid segmentation using elastic regularization, *IEEE Transactions on Pattern Analysis and Machine Intelligence* 42 (12) (2020) 3054–3070.
 - [40] D. Ren, W. Zuo, D. Zhang, L. Zhang, M.-H. Yang, Simultaneous fidelity and regularization learning for image restoration, *IEEE Transactions on Pattern Analysis and Machine Intelligence* 43 (1) (2021) 284–299.
 - [41] P. Luo, R. Zhang, J. Ren, Z. Peng, J. Li, Switchable normalization for learning-to-normalize deep representation, *IEEE Transactions on Pattern Analysis and Machine Intelligence* 43 (2) (2021) 712–728.
 - [42] X. Pan, P. Luo, J. Shi, X. Tang, Two at once: Enhancing learning and generalization capacities via ibn-net, in: *Proceedings of the European Conference on Computer Vision (ECCV)*, 2018, pp. 464–479.
 - [43] Y. Wu, K. He, Group normalization, in: *Proceedings of the European conference on computer vision (ECCV)*, 2018, pp. 3–19.
 - [44] L. Huang, X. Liu, Y. Liu, B. Lang, D. Tao, Centered weight normalization in accelerating training of deep neural networks, in: *Proceedings of the IEEE International Conference on Computer Vision (ICCV)*, 2017, pp. 2803–2811.
 - [45] B. Zhao, X. Zhang, Z. Li, X. Hu, A multi-scale strategy for deep semantic segmentation with convolutional neural networks, *Neurocomputing* 365 (2019) 273–284.
 - [46] M. Hao, Y. Liu, X. Zhang, J. Sun, Labelenc: A new intermediate supervision method for object detection, in: *Proceedings of the European Conference on Computer Vision (ECCV)*, 2020, pp. 529–545.
 - [47] J. Sun, Y. Shen, W. Yang, Q. Liao, Classifier shared deep network with multi-hierarchy loss for low resolution face recognition, *Signal Processing: Image Communication* 82 (2020) 115766.
 - [48] J. Wang, K. Sun, T. Cheng, B. Jiang, C. Deng, Y. Zhao, D. Liu, Y. Mu, M. Tan, X. Wang, et al., Deep high-resolution representation learning for visual recognition, *IEEE Transactions on Pattern Analysis and Machine Intelligence* 0 (2020) 1–16. doi:10.1109/TPAMI.2020.2983686.
 - [49] Y. Zhang, Y. Tian, Y. Kong, B. Zhong, Y. Fu, Residual dense network for image restoration, *IEEE Transactions on Pattern Analysis and Machine Intelligence* 0 (2020) 1–16. doi:10.1109/TPAMI.2020.2968521.
 - [50] D. Avola, M. Cascio, L. Cinque, A. Fagioli, G. L. Foresti, C. Massaroni, Master and rookie networks for person re-identification, in: *Proceedings of the International Conference on Computer Analysis of Images and Patterns (CAIP)*, 2019, pp. 470–479.
 - [51] K. Simonyan, A. Zisserman, Very deep convolutional networks for large-scale image recognition, *arXiv preprint arXiv:1409.1556* 0 (2014) 1–14.
 - [52] V. Dumoulin, F. Visin, A guide to convolution arithmetic for deep learning, *arXiv preprint arXiv:1603.07285* 0 (2016) 1–32.
 - [53] A. Krizhevsky, G. Hinton, et al., Learning multiple layers of features from tiny images, *Technical Report* 0 (2009) 1–58.
 - [54] T. DeVries, G. W. Taylor, Improved regularization of convolutional neural networks with cutout, *arXiv preprint arXiv:1708.04552* 0 (2017) 1–8.